View metadata, citation and similar papers at core.ac.uk

brought to you by CORE

provided by eResearch@Ozyegin

Credible Intervals for Nanoparticle Characteristics

Richard Charnigo[a,*], Mathieu Francoeur[b], Patrick Kenkel[a],

M. Pinar Mengüç[c], Benjamin Hall[a], and Cidambi Srinivasan[a]

[a] Department of Statistics, 817 Patterson Office Tower

University of Kentucky, Lexington KY USA 40506-0027

E-Mail: RJCharn2@aol.com, kenkel.kenkel@gmail.com,

Benjamin.Hall@uky.edu, srini@ms.uky.edu

[b] Department of Mechanical Engineering, 50 S. Central Campus Drive

MEB 2126, University of Utah, Salt Lake City UT USA 84112

E-Mail: mfrancoeur@mech.utah.edu

[c] Department of Mechanical Engineering,

Ozyegin University, Cekmekoy İstanbul Turkey

E-Mail: pinar.menguc@ozyegin.edu.tr

[*] Corresponding Author

Phone: 859.257.5678 x82072, Fax: 859.257.6430, E-Mail: RJCharn2@aol.com

Abstract

Solving the inverse problem of nanoparticle characterization has the potential to advance science and benefit society. While considerable progress has been made within a framework based on the scattering of surface plasmon-polaritons, an aspect not heretofore considered is the quantification of uncertainty in the estimation of a nanoparticle characteristic. Therefore, the present article offers a technique by which an investigator may augment an estimate of a nanoparticle characteristic with a companion "credible interval". Analogous to the familiar confidence interval but arising from within the Bayesian statistical paradigm, a credible interval allows the investigator to make a statement such as "the nanoparticle diameter lies between 36 and 48 nm with 95% probability" instead of merely "the nanoparticle diameter is estimated to be 42 nm". Our technique may even be applied outside of the surface plasmon-polariton scattering framework, as long as the investigator specifies his/her prior beliefs about the nanoparticle characteristic and indicates which potential outcomes are likely or unlikely in whatever experiment he/she designs to estimate the nanoparticle characteristic. Two numerical studies illustrate the implementation and performance of our technique in constructing ranges of likely values for nanoparticle diameters and agglomeration levels respectively.

Key words: Bayesian; compound estimation; confidence interval; inverse problem; scattering; sufficient statistic; surface plasmon-polariton.

1 Introduction

Nanoparticle characterization is an interesting and challenging inverse problem from both basic and applied perspectives. While there exist several well-established statistical approaches for addressing an inverse problem, such as logistic regression, classification trees, and discriminant analysis (Ripley, 1996; Hastie, Tibshirani, and Friedman, 2001; Fernandez, 2003), many of

these approaches are geared toward a particular structure for the inverse problem, namely that the value of a categorical outcome variable is to be inferred from a collection of quantitative predictor variables. However, nanoparticle characterization may entail a rather different structure, in which the value of a *quantitative* outcome variable is to be inferred from one or more predictor *functions*.

For example, an investigator may wish to infer the average diameter in a collection of nanoparticles based on their "scattering profile". (If the nanoparticles are homogeneously sized, then one may speak of their diameter unambiguously. However, if the nanoparticles are not homogeneously sized, then one may use their average diameter to summarize the distribution of their sizes. For instance, if the nanoparticle diameters follow a lognormal distribution with parameters $\mu = 2$ and $\sigma = 1$ [Casella and Berger, 2002], then their average diameter is 12.2 nm.) As described in detail elsewhere (Videen et al, 2005; Venkata et al, 2007), a scattering profile quantifies how the nanoparticles disperse surface plasmon-polaritons (SPPs) as a function of the angle from the experimental apparatus at which measurements are taken. One may artificially convert such a quantitative outcome variable into a categorical outcome variable (by asking whether the average diameter is above or below some threshold) and change such a predictor function into quantitative predictor variables (by sampling the scattering profile upon a coarse grid of angles), thus permitting application of well-established statistical approaches. Alternatively and preferably, one may seek a statistical approach specifically intended for the natural structure of the inverse problem.

Recently, Charnigo et al (2011) provided such an approach. Actually, they showed how to use not only a scattering profile but also one or more of its derivatives to estimate a quantitative nanoparticle characteristic, such as the average diameter in a collection of nanoparticles or the agglomeration level, defined as the percentage of single (versus agglomerated) nanoparticles. Their approach does not require the human operator to make any subjective judgments based

on visual perceptions of scattering profiles (or their derivatives) and avoids ad-hoc aspects of top-flight methods for characterizing small (but larger-than-nanosize) particles (Agarwal and Mengüç, 1991; Mengüç and Manickavasagam, 1993). Their numerical studies suggested that, with allowance for both systematic error and stochastic noise in data acquisition, their approach might yield typical errors as small as 2.01 nm and 5.65 percent in estimating nanoparticle diameter and agglomeration level respectively.

Yet, a crucial question remains: How can an investigator describe his/her uncertainty about a quantitative nanoparticle characteristic? Numbers such as 2.01 nm and 5.65 percent are square roots of average squared differences between the estimated and actual values of the characteristics. These numbers can only be calculated if the investigator knows the actual values. While such knowledge is available to those conducting numerical studies to evaluate an approach for characterizing nanoparticles, such knowledge is not generally available in a "real world" setting. So, while an investigator employing the approach of Charnigo et al (2011) may be able to assert that "the estimated nanoparticle diameter is 42 nm", he/she may not be able to declare that "with 95% confidence, the actual nanoparticle diameter is between 36 and 48 nm".

The goal of the present article, therefore, is to provide a technique for answering the crucial question above. Importantly, our technique can be applied when there are multiple sources contributing to the uncertainty about a nanoparticle characteristic. Such sources may include both the ill-posedness of the mathematical inverse problem (i.e., the possibility that nanoparticles with different characteristics may behave similarly) and practical difficulties in an experimental setting (e.g., the potential for systematic error and stochastic noise in data acquisition). While we envisage pairing our technique with the nanoparticle characterization approach of Charnigo et al (2011), our technique is actually rather general. Indeed, there are only three requirements for its use.

First, an investigator must identify the characteristic of interest and specify his/her prior beliefs about what values are likely or unlikely for that characteristic (Step 1 in Section 3). The investigator may also adopt essentially neutral prior beliefs, in a sense to be made precise later. Second, the investigator must identify an experimental framework from which data will be acquired (Step 2). Although we exemplify our technique in the SPP-scattering framework of Videen et al (2005) and Venkata et al (2007), our technique is not restricted to that framework. Third, the investigator must specify which potential outcomes from the experiment are likely or unlikely in relation to the value of the characteristic of interest (Step 3). Fulfilling this third requirement may necessitate some auxiliary experimentation, as described later.

Once these three requirements are met, the investigator ascertains what values are likely or unlikely for the characteristic of interest given the experimental results (Step 4) and then constructs a range of likely values for the characteristic (Step 5). This range is similar to a confidence interval but has a slightly different interpretation due to its connection with the Bayesian statistical paradigm (Gelman et al, 1995; Casella and Berger, 2002). As such, we refer to this range as a "credible interval" instead of as a confidence interval. In summary, our technique allows an investigator to make a statement such as "with 95% probability, the actual nanoparticle diameter is between 36 and 48 nm".

As indicated above, we illustrate our technique in the SPP-scattering framework, which entails analysis of the scattering Mueller matrix elements providing the change of intensity and polarization state of the scattered SPPs. Importantly, our technique is not limited to that framework. Other frameworks to which our technique is potentially applicable include, for example, particle sizing using time-resolved laser-induced incandescence (Daun et al, 2007) and particle characterization via lidar (Muller et al, 2011; Nishizawa et al, 2011). Our technique is also potentially applicable to problems in biomedicine, such as optical tomography (Arridge, 1999; Gu et al, 2009) and fluorescence tomography (Kim et al, 2010). However, for concreteness

and because our research team has a particular interest in nanoparticle characterization via the SPP-scattering framework, we maintain that perspective for the balance of this article.

Indeed, we envisage that nanoparticle characterization may have profound impacts on science and society during the next decade. Nanoparticles may allow for the engineering of structures and devices that possess unique and unprecedented optical, electrical, thermal, or structural properties. In particular, bottom-up fabrication processes would ideally require a robust framework for characterizing nanoparticles nonintrusively and in real time. Metallic nanoparticles may be used to increase the efficiency of photovoltaic cells (Catchpole and Polman, 2008; Atwater and Polman, 2010). Materials comprised of sub-wavelength inclusions, called metamaterials, may lead to unprecedented optical properties such as negative refractive indices. Recently, materials made of dielectric nanoparticles have been investigated to fabricate in a simple manner isotropic metamaterials with engineered electrical permittivity and magnetic permeability (Zhao et al, 2009; Cai and Shalaev, 2010). Moreover, nanoparticles may play a key role in nanoscale-gap thermophotovoltaic (nano-TPV) power generation, where a cell converts thermal radiation from a terrestrial source into electricity (Whale, 1997; DiMatteo et al, 2001; Laroche et al, 2006; Park et al, 2008; Francoeur et al, 2011). Francoeur et al (2011) demonstrated that viable and highly efficient nano-TPV power generators are possible only if the near-field radiative spectrum can be finely tuned at selected wavelengths. Nanoparticles coated on the source or on the cell may allow such a fine tuning of near-field thermal emission and absorption.

In the aforementioned applications of nanoparticles, and in numerous others, nanoparticle characteristics such as shapes, sizes, and agglomeration levels need to be controlled precisely to achieve the desired properties. As such, we believe that the inverse problem of characterizing nanoparticles nonintrusively and in real time is worth solving and, therefore, being able to quantify uncertainty about a nanoparticle characteristic represents a useful methodological

advance.

The rest of this article is organized as follows. Section 2 describes some statistical concepts relevant to the construction of credible intervals for a characteristic of interest such as average nanoparticle diameter or percentage of single nanoparticles. Section 3 presents our five-step technique for constructing credible intervals. Section 4 describes two numerical studies that were performed to assess our technique, in terms of both the lengths of the intervals and the relative frequencies with which the intervals contained the actual value of the characteristic of interest. Section 5 summarizes this article's contributions and highlights some opportunities for future research. Additional details regarding the numerical studies appear in the Appendix. A glossary of notation is provided in Table 1.

2 Statistical Concepts

We describe some statistical concepts relevant to the construction of credible intervals for nanoparticle characteristics. While Section 2 of this article is intended to make the present work self-contained, a reader desiring more details may consult Sections 4.1, 9.2.4, and 6.2.1 of Casella and Berger (2002) along with Sections 1.3 and 2.3 of Gelman et al (1995). Also, to help the reader keep track of the notation introduced in Section 2 of this article, we provide a glossary in Table 1.

2.1 Probability Density Function

Suppose that $\mathbf{Y} = (Y_1, Y_2, \ldots, Y_n)^T$ is an n-dimensional vector of random variables governed by a probability density function $f(\mathbf{y}; u)$. The interpretation of $f(\mathbf{y}; u)$ is that the probability of $\mathbf{Y}$ falling inside A, a subset of n-dimensional space $\mathbb{R}^n$, is obtained by integrating $f(\mathbf{y}; u)$

over A, $P(\mathbf{Y} \in A) = \int_A f(\mathbf{y}; u)\ d\mathbf{y}$. In accord with this interpretation, we must have

$$f(\mathbf{y}; u) \geq 0 \quad \text{and} \quad \int_{\mathbb{R}^n} f(\mathbf{y}; u)\ d\mathbf{y} = 1. \tag{1}$$

The mathematical form of $f(\mathbf{y}; u)$ is sometimes treated as known, but the parameter u is usually regarded as unknown and is thus estimated from the realized values of $Y_1, Y_2, \ldots, Y_n$. (If we observe that $Y_1 = 24$, for instance, then 24 is called the "realized value" of Y_1.) To distinguish the random variables from their realized values, we denote the latter by lower case symbols $y_1, y_2, \ldots, y_n$ (or, collectively, by $\mathbf{y}$) and refer to them as "data".

One example of a probability density function is

$$f(\mathbf{y}; u) = (2\pi)^{-n/2} \exp\left[-\sum_{i=1}^{n} (y_i - u)^2/2\right]. \tag{2}$$

Random variables $Y_1, Y_2, \ldots, Y_n$ governed by (2) are mutually uncorrelated and are normally distributed with mean u and unit standard deviation. In this example, an estimate of u is the "sample mean" $\bar{y} := \sum_{i=1}^{n} y_i/n$.

2.2 Bayesian Credible Interval

In a Bayesian statistical paradigm, the parameter u in the probability density function $f(\mathbf{y}; u)$ is regarded as not only unknown but also random. Our belief about the probabilistic behavior of u before observing the data is summarized by a prior probability density function, denoted $pr(u)$. The interpretation of $pr(u)$ is that $P(u \in B) = \int_B pr(u)\ du$, where B is a subset of the real numbers $\mathbb{R}$.

Bayes' Theorem provides a mechanism for updating our belief about the probabilistic behavior of u after observing the data. More specifically, Bayes' Theorem leads us to define a posterior probability density function as

$$po(u; \mathbf{y}) := \frac{pr(u)\ f(\mathbf{y}; u)}{\int_{\mathbb{R}} pr(v)\ f(\mathbf{y}; v)\ dv}. \tag{3}$$

The interpretation of $po(u;\mathbf{y})$ is that $P(u \in B \mid \mathbf{Y} = \mathbf{y}) = \int_B po(u;\mathbf{y})\ du$. (The left side of the preceding equality may be read as "the probability that u falls inside B given that the realization of $\mathbf{Y}$ is $\mathbf{y}$".)

A 95% Bayesian credible interval (sometimes also called a posterior interval) is analogous to the familiar 95% confidence interval. However, while the familiar confidence interval provides a range of plausible values for u when u is treated as unknown but non-random, a Bayesian credible interval provides a range of likely values for u when u is regarded as unknown and random.

More specifically, a 95% Bayesian credible interval I is a closed subset of $\mathbb{R}$ satisfying

$$\int_I po(u;\mathbf{y})\ du = 0.95. \tag{4}$$

In words, (4) says that I captures u with probability 95% after we observe the data. Note, however, that I is not uniquely determined by (4).

On the other hand, assuming (as is typically true) that $po(u;\mathbf{y})$ is continuous and has a single local maximum with respect to its primary argument, adding a second constraint

$$\inf_{u \in I} po(u;\mathbf{y}) \geq \sup_{u \notin I} po(u;\mathbf{y}) \tag{5}$$

does uniquely determine I. (Above, "inf" and "sup" stand for infimum and supremum, which are defined as the greatest lower bound and the least upper bound of their respective sets. As such, infimum and supremum generalize the concepts of minimum and maximum.) In words, (5) says that I accumulates its 95% probability from likely values of u rather than from unlikely values.

Figure 1 exemplifies a 95% Bayesian credible interval. Satisfaction of (4) corresponds to the shaded area under $po(u;\mathbf{y})$ equaling 0.95. Adherence to (5) is represented by the presence of shading at u values for which $po(u;\mathbf{y}) > 0.08$ and the absence of shading at u values for which $po(u;\mathbf{y}) \leq 0.08$.

2.3 Sufficient Statistic and Dimension Reduction

The probability density function $f(\mathbf{y}; u)$ can sometimes be decomposed into a product of the form $g(t(\mathbf{y}); u)\ h(\mathbf{y})$, where $t(\mathbf{y})$ is of lower dimension than $\mathbf{y}$. Note that $h(\mathbf{y})$ is not permitted to depend on u, while $g(t(\mathbf{y}); u)$ is allowed to depend on $\mathbf{y}$ only through $t(\mathbf{y})$. We refer to such $t(\mathbf{y})$ as a sufficient statistic.

For example, with $f(\mathbf{y}; u)$ as in (2), we can take $t(\mathbf{y}) := \bar{y}$, $g(t(\mathbf{y}); u) := \exp[n\bar{y}u - nu^2/2]$, and $h(\mathbf{y}) := (2\pi)^{-n/2} \exp[-\sum_{i=1}^{n} y_i^2/2]$ to see that the sample mean $\bar{y}$ is a sufficient statistic.

The nomenclature "sufficient" conveys that $t(\mathbf{y})$ is sufficient for estimating u in the sense that $t(\mathbf{y})$ contains all of the information in $\mathbf{y}$ that is relevant to estimating u. Indeed, the posterior probability density function (3) can be expressed as

$$po(u; \mathbf{y}) = \frac{pr(u)\ g(t(\mathbf{y}); u)\ h(\mathbf{y})}{\int_{\mathbb{R}} pr(v)\ g(t(\mathbf{y}); v)\ h(\mathbf{y})\ dv} = \frac{pr(u)\ g(t(\mathbf{y}); u)}{\int_{\mathbb{R}} pr(v)\ g(t(\mathbf{y}); v)\ dv}, \tag{6}$$

revealing that (3) — and, hence, a Bayesian credible interval for u derived from (3) — will depend on the data $\mathbf{y}$ only through the sufficient statistic $t(\mathbf{y})$. In effect, then, a sufficient statistic $t(\mathbf{y})$ reduces the dimension of the data $\mathbf{y}$.

3 Methodology

We now present our approach to obtaining credible intervals for nanoparticle characteristics. For ease of exposition, we present our approach in five steps. As with Section 2, notation introduced herein is recorded in a glossary (Table 1).

Step 1: Define a prior probability density function for the characteristic of interest. Let u denote a quantitative characteristic of interest describing a collection of nanoparticles. For instance, u may be the average diameter of the nanoparticles. In this case, if an investigator's prior belief is that the average diameter is somewhere between 5 nm and 100 nm but that no

values in this range are more likely candidates than others for the average diameter, then the investigator may define the prior probability density function $pr(u)$ to be $1/(100-5) = 1/95$ for $u \in [5, 100]$ and 0 for $u \notin [5, 100]$.

A prior probability density function that is constant when nonzero is called "noninformative" (Cf. Section 2.8 of Gelman et al, 1995). Choosing $pr(u)$ to be noninformative represents an essentially neutral stance for an investigator since $pr(u)$ then factors out of either (3) or (6). In this case, the credible interval is determined only by the data $\mathbf{y}$ or the sufficient statistic $t(\mathbf{y})$.

Step 2: Specify an experimental framework for acquiring the data. Let $\mathbf{Y}$ denote a vector of random variables representing potential outcomes from an experiment designed to aid in nanoparticle characterization. For example, suppose that the experimental paradigm of Videen et al (2005) and Venkata et al (2007) is employed. In this case, the nanoparticles are placed on a metallic film coated on a high refractive index substrate. Elliptically polarized radiation is directed to the interface between the substrate and the metallic film, yielding evanescent waves at the substrate-metal interface. These evanescent waves tunnel through the metallic film and excite surface plasmon-polaritons (SPPs) at the metal-air interface. The SPPs are, in turn, scattered by the nanoparticles. At each of numerous angles in the far field, the change of intensity and polarization state of the scattered SPPs is recorded. One then defines the components of $\mathbf{Y}$ to be normalized entries from the 4×4 scattering Mueller matrix derived from the information recorded in the far field (Bohren and Huffman, 1998). For example, if information is recorded at far field angles between 2 and 178 degrees in increments of 1 degree, then $\mathbf{Y}$ is a vector of length 177 whose i^{th} component Y_i is a normalized entry from the scattering Mueller matrix based on the information recorded at a far field angle of $(i+1)$ degrees for $i \in \{1, 2, \ldots, 177\}$. (The process of normalizing entries from the scattering Mueller matrix is described in the last paragraph of Section 2 in Charnigo et al (2007), while Figure 1

in Charnigo et al (2011) displays a visual schematic of the experimental paradigm.)

Step 3: Identify likely and unlikely potential outcomes from the experiment. Ideally, an investigator would be able to specify a probability density function $f(\mathbf{y}; u)$ identifying which potential outcomes from the experiment were likely or unlikely in relation to the characteristic of interest. However, the correct mathematical form of $f(\mathbf{y}; u)$ might not be apparent from physical principles. At least conceptually, there are three possible avenues by which the investigator might address this difficulty.

Avenue 1: Nonparametric estimation of the probability density function. In this first avenue, the investigator would not speculate about the correct mathematical form of $f(\mathbf{y}; u)$. Indeed, as the investigator proceeded to estimate $f(\mathbf{y}; u)$, no assumption would be made other than (1).

Toward estimating $f(\mathbf{y}; u)$, the investigator could conduct auxiliary experiments using different collections of nanoparticles for which the investigator knew the characteristic of interest. For example, if the characteristic of interest were average diameter, then the investigator could run M (a positive integer) auxiliary experiments using nanoparticles with average diameter known to equal 5 nm. This would yield M auxiliary data sets from which the investigator could estimate $f(\mathbf{y}; 5)$ using a nonparametric density estimation method (Loader, 1999; Devroye and Lugosi, 2001), which would not make any assumption other than (1). (Above, the substitution of 5 for u in $f(\mathbf{y}; u)$ indicates that the probability density function is being estimated based on nanoparticles for which the average diameter is known to equal 5 nm.)

Continuing, the investigator could then run M more auxiliary experiments using nanoparticles with average diameter known to equal 10 nm. This would yield M more auxiliary data sets from which the investigator could estimate $f(\mathbf{y}; 10)$ using a nonparametric density estimation method. The investigator could likewise estimate $f(\mathbf{y}; 15)$, $f(\mathbf{y}; 20)$, and so forth. Interpolation

could be used to complete the estimation of $f(\mathbf{y}; u)$ for any value of u not represented in the auxiliary experiments. For instance, an estimate of $f(\mathbf{y}; 6)$ could be defined as 1/5 the estimate of $f(\mathbf{y}; 10)$ plus 4/5 the estimate of $f(\mathbf{y}; 5)$.

While defensible conceptually, this avenue suffers from the practical difficulty that, at any fixed value of u, $f(\mathbf{y}; u)$ is a function with domain a subset of n-dimensional space $\mathbb{R}^n$. Adequately estimating such a function using a nonparametric density estimation method would require M to greatly exceed n. Thus, unless n were quite small, thousands of auxiliary experiments would be required at any fixed value of u.

Avenue 2: Parametric estimation of the probability density function. The investigator might be willing to assume that $f(\mathbf{y}; u)$ could be approximated by a probability density function of known mathematical form. One example would be the n-dimensional normal probability density function with $n \times 1$ mean vector $\mu(u)$ and symmetric, positive definite $n \times n$ covariance matrix $\Sigma(u)$,

$$(2\pi)^{-n/2} Det[\Sigma(u)]^{-1/2} \exp[-(\mathbf{y} - \mu(u))^T \Sigma(u)^{-1} (\mathbf{y} - \mu(u))/2], \tag{7}$$

where $Det[\cdot]$ returns the determinant of a matrix. (Expression (2) is a special case of expression (7) in which every component of $\mu(u)$ is restricted to equal u and $\Sigma(u)$ is taken to be an identity matrix.)

The components of $\mu(u)$ and $\Sigma(u)$ could then be estimated from auxiliary experiments using different collections of nanoparticles for which the investigator knew the characteristic of interest. For example, if the characteristic of interest were average diameter, then the investigator could run M auxiliary experiments using nanoparticles with average diameter known to equal 5 nm. This would yield M auxiliary data sets from which the investigator could estimate the components of $\mu(5)$ and $\Sigma(5)$ by a parametric statistical technique such as the method of moments (Cf. Section 7.2.1 of Casella and Berger, 2002). (Here the substitution of 5 for u in $\mu(u)$ and $\Sigma(u)$ indicates estimation based on nanoparticles for which the average

diameter is known to equal 5 nm.) The investigator could likewise estimate $\mu(10)$, $\Sigma(10)$, $\mu(15)$, $\Sigma(15)$, and so forth. Interpolation could be used to estimate the components of $\mu(u)$ and $\Sigma(u)$ for any value of u not represented in the auxiliary experiments.

This second avenue involves a tradeoff between realism and practicality. If no restrictions were imposed a priori on $\mu(u)$ and $\Sigma(u)$ (other than symmetry and positive definiteness of the latter), then a realistic approximation to $f(\mathbf{y};u)$ might be possible. However, there would be on the order of $n^2/2$ components to estimate. This would not provide a viable alternative to the first avenue, since again thousands of auxiliary experiments would be required at any fixed value of u. On the other hand, imposing restrictions on $\mu(u)$ and $\Sigma(u)$ could drastically reduce the number of components to estimate. The number of required auxiliary experiments would then also be reduced. Yet, such restrictions might preclude a realistic approximation to $f(\mathbf{y};u)$.

Avenue 3: Dimension reduction followed by parametric estimation. Not knowing the mathematical form of $f(\mathbf{y};u)$ impedes the identification of a sufficient statistic $t(\mathbf{y})$. However, an investigator may identify a quantity $\widetilde{t}(\mathbf{y})$ that he/she is willing to treat like a sufficient statistic in that he/she will rely on $\widetilde{t}(\mathbf{y})$ to obtain credible intervals for nanoparticle characteristics. Thus, the investigator will still be reducing the dimension of the data $\mathbf{y}$.

For example, if the characteristic of interest were average diameter and one employed the experimental paradigm of Videen et al (2005) and Venkata et al (2007), then one might put

$$\widetilde{t}(\mathbf{y}) := (\log D(\mathbf{y};10), \log D(\mathbf{y};50), \log D(\mathbf{y};90))^T, \quad \text{where} \tag{8}$$

$$\begin{aligned} D(\mathbf{y};c) \;:=\; & 0.9362\ \frac{\int_0^{180}[M_{33}(\theta;\mathbf{y}) - M_{33;c}(\theta)]^2\ d\theta}{\int_0^{180} M_{33}(\theta;\mathbf{y})^2\ d\theta} + 0.0466\ \frac{\int_0^{180}[M'_{33}(\theta;\mathbf{y}) - M'_{33;c}(\theta)]^2\ d\theta}{\int_0^{180} M'_{33}(\theta;\mathbf{y})^2\ d\theta} \\ & +0.0172\ \frac{\int_0^{180}[M''_{33}(\theta;\mathbf{y}) - M''_{33;c}(\theta)]^2\ d\theta}{\int_0^{180} M''_{33}(\theta;\mathbf{y})^2\ d\theta}. \end{aligned} \tag{9}$$

Above, $M_{33}(\theta;\mathbf{y})$ represents an estimate of the normalized entry from the third row and third column of the scattering matrix, as a function of the far field angle θ, for nanoparticles of

unknown average diameter from which data $\mathbf{y}$ are generated. Note that $M_{33}(\theta;\mathbf{y})$ is, in essence, a smooth connection of the dots formed by plotting $y_1,\ldots,y_n$ against their corresponding far field angles. Figure 2 displays a visual schematic of this smoothing, which is based on the compound estimation procedure of Charnigo and Srinivasan (2011a, 2011b).

Continuing, $M_{33;c}(\theta)$ is analogous to $M_{33}(\theta;\mathbf{y})$ but pertains to nanoparticles of known average diameter c. The primes denote differentiation with respect to θ. The coefficients 0.9362, 0.0466, and 0.0172 were identified as optimal for estimating average diameter in a numerical study by Charnigo et al (2011). More specifically, the root mean square error in estimating average diameter by $\arg\min_c D(\mathbf{y};c)$ was smallest when $D(\mathbf{y};c)$ was defined with these coefficients, assuming low stochastic noise in the process generating the data $\mathbf{y}$.

The rationale for (8) is that small $D(\mathbf{y};10)$ but large $D(\mathbf{y};50)$ and $D(\mathbf{y};90)$ will suggest that the unknown average diameter may be close to 10 nm, small $D(\mathbf{y};50)$ but large $D(\mathbf{y};10)$ and $D(\mathbf{y};90)$ will suggest that the unknown average diameter may be close to 50 nm, medium $D(\mathbf{y};10)$ and $D(\mathbf{y};50)$ but large $D(\mathbf{y};90)$ will suggest that the unknown average diameter may be close to 30 nm, and so forth. Thus, $D(\mathbf{y};10)$, $D(\mathbf{y};50)$, and $D(\mathbf{y};90)$ are potentially quite informative for estimating the unknown average diameter.

Once $\widetilde{t}(\mathbf{y})$ has been chosen, the investigator must specify $g(\widetilde{t}(\mathbf{y});u)$ for use in the formula

$$po(u;\mathbf{y}) \approx \frac{pr(u)\ g(\widetilde{t}(\mathbf{y});u)}{\int_{\mathbb{R}} pr(v)\ g(\widetilde{t}(\mathbf{y});v)\ dv}, \tag{10}$$

which modifies formula (6) above only in that $g(t(\mathbf{y});u)$ has been replaced by $g(\widetilde{t}(\mathbf{y});u)$. One possibility is to assign $g(\widetilde{t}(\mathbf{y});u)$ to have the form

$$(2\pi)^{-dim[\widetilde{t}(\mathbf{y})]/2} Det[\Lambda(u)]^{-1/2} \exp[-(\widetilde{t}(\mathbf{y})-\nu(u))^T \Lambda(u)^{-1} (\widetilde{t}(\mathbf{y})-\nu(u))/2], \tag{11}$$

where $dim[\cdot]$ returns the dimension of a vector, $\nu(u)$ is a $dim[\widetilde{t}(\mathbf{y})] \times 1$ mean vector, and $\Lambda(u)$ is a symmetric, positive definite $dim[\widetilde{t}(\mathbf{y})] \times dim[\widetilde{t}(\mathbf{y})]$ covariance matrix.

The components of $\nu(u)$ and $\Lambda(u)$ could then be estimated from auxiliary experiments using different collections of nanoparticles for which the investigator knew the characteristic of

interest. If $\widetilde{t}(\mathbf{y})$ were chosen as in (8), so that $dim[\widetilde{t}(\mathbf{y})] = 3$, then even without imposing any restrictions on $\nu(u)$ and $\Lambda(u)$ (other than symmetry and positive definiteness of the latter) there would be only nine components to estimate. That could be accomplished with a comparatively modest number of auxiliary experiments, rendering this third avenue more feasible than the first two. As such, we pursue this third avenue in our numerical studies (Section 4).

Step 4: Conduct the experiment and obtain the posterior probability density function for the characteristic of interest. When the investigator applies the experimental framework from Step 2 to a collection of nanoparticles with unknown characteristic, the investigator will acquire data $\mathbf{y}$ and, presuming pursuit of the third avenue in Step 3, the dimension-reduced quantity $\widetilde{t}(\mathbf{y})$. Then, using the prior probability density function $pr(u)$ specified in Step 1, the investigator may obtain the (approximate) posterior probability density function $po(u; \mathbf{y})$ via formula (10).

Step 5: Derive the credible interval for the characteristic of interest. Once the (approximate) posterior probability density function $po(u; \mathbf{y})$ has been obtained, a(n approximate) 95% Bayesian credible interval may be derived by meeting requirements (4) and (5) simultaneously. One computational procedure for doing so follows.

First, express $C := \{u \in \mathbb{R} : pr(u) > 0\}$ as a finite union of numerous short intervals, $C = [a_0, a_1] \cup [a_1, a_2] \cup \ldots \cup [a_{k-1}, a_k]$ for some positive integer k. These short intervals should conform to a tolerable level of rounding for the endpoints of the credible interval. For example, if the characteristic of interest is average diameter and the investigator is willing to round the endpoints of the credible interval to the nearest nm, then with $C = [5, 100]$ the investigator may take $k := 95$ and $a_j := j + 5$ for $j \in \{0, 1, \ldots, k\}$.

Next, put $N_j := pr(a_j)\ g(\widetilde{t}(\mathbf{y}); a_j)$ for $j \in \{0, 1, \ldots, k\}$. Observe that N_j is the numerator of (10) evaluated at $u = a_j$. Also, let τ be a permutation of $\{0, 1, \ldots, k\}$ such that $N_{\tau[0]} \geq$

$N_{\tau[1]} \geq \ldots \geq N_{\tau[k]}$. In words, τ sorts $N_0, N_1, \ldots, N_k$ in order from largest to smallest. To illustrate this sorting, we again consider Figure 1. Let k and a_j be as in the last line of the preceding paragraph. We have $\tau[0] = 23$ in accord with the numerator of the posterior probability density function (and, hence, the posterior probability density function itself) being maximized at $u = a_{23} = 28$. We also have $\tau[1] = 24$, $\tau[2] = 22$, and so forth.

Then, identify the smallest nonnegative integer m such that

$$\frac{\sum_{j=0}^{m} N_{\tau[j]}}{\sum_{j=0}^{k} N_j} \geq 0.95. \tag{12}$$

The credible interval is the smallest interval containing $\{a_{\tau[0]}, a_{\tau[1]}, \ldots, a_{\tau[m]}\}$. Note that condition (12) corresponds to requirement (4), while sorting via τ addresses requirement (5).

4 Numerical Studies

We describe two numerical studies that were conducted to evaluate our approach to constructing credible intervals, in terms of both the lengths of the intervals and the relative frequencies with which the intervals contained the actual value of the nanoparticle characteristic of interest. The first numerical study pertained to the estimation of nanoparticle diameter, while the second entailed the estimation of agglomeration level.

4.1 Credible Intervals for Nanoparticle Diameter

Our first numerical study was performed to assess our approach to obtaining credible intervals for nanoparticle diameter in a collection of homogeneously sized nanoparticles, allowing for both systematic error and stochastic noise in data acquisition. The study design is described in detail below, in parallel with the five steps of Section 3, after which we present our findings.

Step 1. Here u represents nanoparticle diameter. We specified a noninformative prior probability density function $pr(u) := 1/95$ for $u \in [5, 100]$ and 0 for $u \notin [5, 100]$.

Step 2. We used the Venkata et al (2007) Fortran implementation of the Videen et al (2005) and Venkata et al (2007) experimental paradigm (along with the rnorm function in the R statistical software package) to generate data sets $\mathbf{y}_{11,u,rep}$, $\mathbf{y}_{12,u,rep}$, $\mathbf{y}_{33,u,rep}$, and $\mathbf{y}_{34,u,rep}$ for $u \in \{5, 10, \ldots, 100\}$ and $rep \in \{1, 2, \ldots, 140\}$. Each data set, representing a realized experimental outcome, contained normalized entries from the scattering matrix corresponding to far field angles of $2, 3, \ldots, 178$ degrees. Each data set was subsequently (Step 5) used to construct a credible interval for nanoparticle diameter.

The underlying physical attributes of the nanoparticles and experimental apparatus were as follows: radiation beam with wavelength 514.5 nm (argon-ion laser) and 23-degree angle of incidence; prism and substrate made of sapphire with refractive index 1.77304; substrate coated with 20 nm gold film having complex refractive index $0.50 + 1.86i$; gold spherical nanoparticles having complex refractive index $0.50 + 1.86i$; 50 percent single nanoparticles and 50 percent agglomerated nanoparticles. Detailed assumptions about agglomeration patterns are documented in the Appendix; however, knowledge of that material is not necessary for the reader to understand what follows.

The 11, 12, 33, and 34 subscripts in our notation identify the row and column of the scattering matrix from which entries were taken. Previous work (Francoeur, Venkata, and Mengüç, 2007; Manickavasagam and Mengüç, 1997) suggests that entries from these rows and columns may be most useful for nanoparticle characterization.

The u index ranging through $\{5, 10, \ldots, 100\}$ indicates that some of the data sets were generated corresponding to nanoparticles with diameter 5 nm, some were generated corresponding to nanoparticles with diameter 10 nm, and so forth.

The *rep* index ranging through $\{1, 2, \ldots, 140\}$ indicates that there were 140 ($= 10 \times 14$) "repetitions" of data generation at each nanoparticle diameter. More specifically, there were 10 repetitions corresponding to each of the following 14 systematic errors: (1) 24-degree angle of incidence; (2) 22-degree angle of incidence; (3) 25-degree angle of incidence; (4) 21-degree angle of incidence; (5) +1 degree offset in measurement angle; (6) -1 degree offset in measurement angle; (7) 3-degree solid angle in far field measurement; (8) 21-degree angle of incidence, +1 degree offset in measurement angle; (9) 25-degree angle of incidence, -1 degree offset in measurement angle; (10) incident beam spread over a solid angle (23 and 24 degrees); (11) incident beam spread over a solid angle (23 and 24 degrees), 3-degree solid angle in far field measurement; (12) incident beam spread over a solid angle (22, 23, and 24 degrees), 2-degree solid angle in far field measurement; (13) incident beam spread over a solid angle (22 and 23 degrees), +1 degree offset in measurement angle; and, (14) incident beam spread over a solid angle (22 and 23 degrees), -1 degree offset in measurement angle.

The 10 repetitions corresponding to any particular systematic error differed among themselves in that they entailed various realizations of stochastic noise. More specifically, each repetition was defined through the addition of stochastic noise from a Gaussian distribution having mean 0 and standard deviation equal to 3% of the standard deviation of the scattering matrix entries, as calculated prior to the addition of stochastic noise.

Step 3. As noted in Section 3, we pursued the third avenue for identifying likely and unlikely potential outcomes: dimension reduction followed by parametric estimation.

Let $\mathbf{y}$ denote any one of the data sets $\mathbf{y}_{33,u,rep}$, $u \in \{5, 10, \ldots, 100\}$ and $rep \in \{1, 2, \ldots, 140\}$, containing entries from the third row and third column of the scattering matrix. We employed the compound estimation procedure of Charnigo and Srinivasan (2011a, 2011b) to convert $\mathbf{y}$ to a smooth curve $M_{33}(\theta; \mathbf{y})$, as illustrated in Figure 2. Implementation details for compound

estimation are documented in the Appendix; however, knowledge of that material is not necessary for the reader to understand what follows.

We then applied the Venkata et al (2007) Fortran implementation three more times to generate entries from the scattering matrix for nanoparticles with diameters 10, 50, and 90 nm respectively, without any systematic errors or stochastic noise. Compound estimation was employed to convert these entries to smooth curves $M_{33}(\theta;10)$, $M_{33}(\theta;50)$, and $M_{33}(\theta;90)$.

We defined $\widetilde{t}(\mathbf{y})$, $D(\mathbf{y};c)$, and $g(\widetilde{t}(\mathbf{y});u)$ as in (8), (9), and (11) respectively. Since the components of $\nu(u)$ and $\Lambda(u)$ in (11) had to be estimated, we generated auxiliary data sets $\mathbf{y}^{aux}_{33,u,rep}$, $u \in \{5,10,\ldots,100\}$ and $rep \in \{1,2,\ldots,70\}$. The auxiliary data sets $\mathbf{y}^{aux}_{33,u,rep}$ were generated in the same manner as the data sets $\mathbf{y}_{33,u,rep}$ from which credible intervals were to be constructed, except that the auxiliary data sets $\mathbf{y}^{aux}_{33,u,rep}$ were fewer in number: at each nanoparticle diameter, there were only 5 repetitions corresponding to each of the 14 systematic errors. The components of $\nu(u)$ and $\Lambda(u)$ were estimated from the auxiliary data sets $\mathbf{y}^{aux}_{33,u,rep}$ by the parametric statistical technique of method of moments.

The above three paragraphs pertain to estimation of nanoparticle diameter based on entries from the third row and third column of the scattering matrix. For entries from other rows and columns, we proceeded similarly except that the coefficients 0.9362, 0.0466, 0.0172 in (9) were modified to accord with the results of Charnigo et al (2011). More specifically, we used coefficients 0.8808, 0, 0.1192 when estimating nanoparticle diameter based on entries from the first row and first column, coefficients 0.4994, 0.4994, 0.0012 for the first row and second column, and coefficients 0.8808, 0.1192, 0 for the third row and fourth column.

Step 4. For each data set $\mathbf{y}_{33,u,rep}$, $u \in \{5,10,\ldots,100\}$ and $rep \in \{1,2,\ldots,140\}$, we calculated a corresponding dimension-reduced quantity $\widetilde{t}(\mathbf{y}_{33,u,rep})$ and, via formula (10), a corresponding posterior probability density function $po(u;\mathbf{y}_{33,u,rep})$. We likewise obtained

$po(u; \mathbf{y}_{11,u,rep})$, $po(u; \mathbf{y}_{12,u,rep})$, and $po(u; \mathbf{y}_{34,u,rep})$ for $u \in \{5, 10, \ldots, 100\}$ and $rep \in \{1, 2, \ldots, 140\}$.

Step 5. From each posterior probability density function $po(u; \mathbf{y}_{33,u,rep})$, $u \in \{5, 10, \ldots, 100\}$ and $rep \in \{1, 2, \ldots, 140\}$, we obtained a 95% Bayesian credible interval $I_{\mathbf{y}_{33,u,rep}}$. The computational procedure described in Section 3 was used with $k := 95$ and $a_j := j + 5$ for $j \in \{0, 1, \ldots, k\}$. We similarly acquired $I_{\mathbf{y}_{11,u,rep}}$, $I_{\mathbf{y}_{12,u,rep}}$, and $I_{\mathbf{y}_{34,u,rep}}$ for $u \in \{5, 10, \ldots, 100\}$ and $rep \in \{1, 2, \ldots, 140\}$.

The findings from this numerical study appear in Figure 3. The circular symbols in panel (a) show $(1/140) \sum_{rep=1}^{140} [\sup I_{\mathbf{y}_{11,5,rep}} - \inf I_{\mathbf{y}_{11,5,rep}}]$, $(1/140) \sum_{rep=1}^{140} [\sup I_{\mathbf{y}_{11,10,rep}} - \inf I_{\mathbf{y}_{11,10,rep}}]$, and so forth. In words, these are the averaged (over 140 repetitions) lengths of the credible intervals $I_{\mathbf{y}_{11,u,rep}}$ corresponding to actual nanoparticle diameters of 5 nm, to actual nanoparticle diameters of 10 nm, and so forth. The square, diamond, and triangular symbols pertain to $I_{\mathbf{y}_{12,u,rep}}$, $I_{\mathbf{y}_{33,u,rep}}$, and $I_{\mathbf{y}_{34,u,rep}}$ respectively.

The credible intervals $I_{\mathbf{y}_{33,u,rep}}$ tend to be narrower than $I_{\mathbf{y}_{11,u,rep}}$ and $I_{\mathbf{y}_{12,u,rep}}$ at all diameters and narrower than $I_{\mathbf{y}_{34,u,rep}}$ at diameters less than 75 nm. Averaging over the 20 actual nanoparticle diameters as well as the 140 repetitions at each diameter, we find that the mean length of the 2800 credible intervals $I_{\mathbf{y}_{33,u,rep}}$ is 3.53 nm, compared to 7.77, 8.94, and 6.84 for $I_{\mathbf{y}_{11,u,rep}}$, $I_{\mathbf{y}_{12,u,rep}}$, and $I_{\mathbf{y}_{34,u,rep}}$ respectively.

The circular symbols in panel (b) of Figure 3 depict $(1/140) \sum_{rep=1}^{140} \mathcal{I}[5 \in I_{\mathbf{y}_{11,5,rep}}]$, $(1/140) \sum_{rep=1}^{140} \mathcal{I}[10 \in I_{\mathbf{y}_{11,10,rep}}]$, and so forth, where $\mathcal{I}$ is an indicator function that equals 1 if its argument is a true statement and 0 otherwise. In words, these are the relative frequencies with which the credible intervals $I_{\mathbf{y}_{11,u,rep}}$ capture the actual nanoparticle diameters (i.e., contain the number 5 when the actual nanoparticle diameters are 5 nm, the number 10 when the actual nanoparticle diameters are 10 nm, and so forth). The square, diamond, and triangular

symbols pertain to $I_{\mathbf{y}_{12,u,rep}}$, $I_{\mathbf{y}_{33,u,rep}}$, and $I_{\mathbf{y}_{34,u,rep}}$ respectively.

Except for $I_{\mathbf{y}_{12,u,rep}}$ at diameters between 75 and 85 nm, all capture rates are at least 90%. Averaging over the 20 actual nanoparticle diameters as well as the 140 repetitions at each diameter, we find that the overall capture rate for $I_{\mathbf{y}_{33,u,rep}}$ is 98.8% compared to 95.8%, 95.0%, and 97.5% for $I_{\mathbf{y}_{11,u,rep}}$, $I_{\mathbf{y}_{12,u,rep}}$, and $I_{\mathbf{y}_{34,u,rep}}$ respectively. Since the intervals were constructed to have 95% credibility, these overall capture rates are satisfactory.

To summarize, entries from the third row and third column of the scattering matrix appear most useful for characterizing nanoparticles of unknown diameter, although other entries may also be suitable for this purpose.

4.2 Credible Intervals for Agglomeration Level

We performed a second numerical study to assess our approach to acquiring credible intervals for agglomeration level in a collection of homogeneously sized nanoparticles.

The design of the first numerical study was largely retained, with agglomeration level replacing nanoparticle diameter as the nanoparticle characteristic of interest. However, since agglomeration level can range from 0 to 100 percent, some minor modifications were made to the study design. For instance, we put $pr(u) := 1/100$ for $u \in [0, 100]$ and 0 for $u \notin [0, 100]$, and actual agglomeration levels in the data sets $\mathbf{y}_{11,u,rep}$, $\mathbf{y}_{12,u,rep}$, $\mathbf{y}_{33,u,rep}$, and $\mathbf{y}_{34,u,rep}$ were taken from among $\{0, 5, \ldots, 100\}$ rather than from among $\{5, 10, \ldots, 100\}$. Meanwhile, nanoparticle diameter was fixed at 50 nm.

Also, in accord with the results of Charnigo et al (2011), the coefficients in quantity (9) were set to 1, 0, 0 when estimating agglomeration level based on entries from the first row and first column of the scattering matrix, to 0.0024, 0.9503, 0.0473 for the first row and second column, to 0, 1, 0 for the third row and third column, and to 1, 0, 0 for the third row and fourth column.

The findings from this numerical study appear in Figure 4. As shown in panel (a), the credible intervals $I_{\mathbf{y}11,u,rep}$ tend to be much wider than $I_{\mathbf{y}12,u,rep}$, $I_{\mathbf{y}33,u,rep}$, and $I_{\mathbf{y}34,u,rep}$ at agglomeration levels above 5 percent. Averaging over all 21 actual agglomeration levels as well as the 140 repetitions at each agglomeration level, we find that the mean length of the 2940 credible intervals $I_{\mathbf{y}11,u,rep}$ is 56.3 percent compared to 17.1, 15.1, and 16.7 percent for $I_{\mathbf{y}12,u,rep}$, $I_{\mathbf{y}33,u,rep}$, and $I_{\mathbf{y}34,u,rep}$ respectively. The extreme width of the credible intervals $I_{\mathbf{y}11,u,rep}$ suggests that entries from the first row and first column of the scattering matrix are not useful for characterizing nanoparticles of unknown agglomeration level.

As depicted in panel (b), the capture rates for $I_{\mathbf{y}33,u,rep}$ fall below 90% at agglomeration levels between 10 and 65 percent as well as between 80 and 90 percent, while the capture rates for $I_{\mathbf{y}34,u,rep}$ fall below 80% at agglomeration levels between 55 and 85 percent. The overall capture rates are 94.7%, 93.9%, 86.8%, and 83.8% for $I_{\mathbf{y}11,u,rep}$, $I_{\mathbf{y}12,u,rep}$, $I_{\mathbf{y}33,u,rep}$, and $I_{\mathbf{y}34,u,rep}$ respectively. The 94.7% and 93.9% are acceptable, whereas the 86.8% and 83.8% are undesirably low. This finding suggests that the statistical model implicit in specification (11) may not be realistic when characterizing nanoparticles of unknown agglomeration level based on entries from the third row and third column or third row and fourth column of the scattering matrix. On the other hand, the statistical model appears adequate for entries from the first row and second column of the scattering matrix.

To summarize, entries from the first row and second column of the scattering matrix appear most useful for characterizing nanoparticles of unknown agglomeration level. While entries from the third row and third column or third row and fourth column have some ability to characterize nanoparticles of unknown agglomeration level, they are not ideal for this purpose due to their lower-than-anticipated capture rates.

5 Discussion

We have presented a technique for quantifying uncertainty about a nanoparticle characteristic when that characteristic is to be inferred from experimental data. Our technique yields a "credible interval", which is the Bayesian statistical paradigm's analogue to the familiar confidence interval. For example, a credible interval of 36 to 48 nm for a nanoparticle diameter indicates that, given the experimental data, there is a 95% chance of the nanoparticle diameter falling between 36 and 48 nm.

While we have illustrated our technique within the SPP-scattering framework of Videen et al (2005) and Venkata et al (2007) involving the scattering Mueller matrix elements, our technique can also be applied with other frameworks as mentioned in Section 1. The performance of our technique with other frameworks will, of course, depend on the extent to which nanoparticles with different characteristics exhibit different behaviors in those frameworks. For instance, if nanoparticles of diameter 10 nm exhibit almost the same behavior as nanoparticles of diameter 50 nm in a particular framework, then applying our technique with that framework may yield rather wide credible intervals for nanoparticle diameter. Thus, selecting a framework that is sensitive to the nanoparticle characteristic of interest is desirable.

Once the investigator has selected such a framework, he/she can employ our technique by specifying each of two key ingredients, namely $pr(u)$ and $f(\mathbf{y};u)$. The former key ingredient reflects the investigator's prior beliefs about the characteristic, while the latter expresses which potential outcomes from the experiment are likely or unlikely. If the investigator does not wish to impose any prior beliefs other than that the characteristic must fall within some interval, then he/she may simply choose $pr(u)$ to be constant on that interval. We have also shown how to apply our technique in the absence of an obvious specification for $f(\mathbf{y};u)$. In this case, the investigator may perform auxiliary experiments to estimate a function $g(\widetilde{t}(\mathbf{y});u)$ that replaces $f(\mathbf{y};u)$ in the derivation of the credible interval.

Our first numerical study demonstrated that, within the SPP-scattering framework, entries from the third row and third column of the scattering matrix could be used to construct credible intervals of average length 3.53 nm for the diameter in a collection of homogeneously sized nanoparticles, without the invocation of informative prior beliefs. Our second numerical study revealed that entries from the first row and second column of the scattering matrix could be employed to acquire credible intervals of average length 17.1 percent for the agglomeration level. Moreover, 98.8% and 93.9% of these credible intervals captured their targets (i.e., actual nanoparticle diameters or actual agglomeration levels), in approximate concordance with their nominal 95% probability levels.

A desirable extension of our technique will entail developing a credible set for a vector of nanoparticle characteristics. For instance, an investigator may wish to make assertions about nanoparticle diameter and agglomeration level simultaneously. Merely defining the credible set for these two characteristics to be the rectangle formed from their respective 95% credible intervals will not suffice: the probability of both characteristics falling within such a rectangle will be somewhat less than 95% and perhaps as low as 90%. To circumvent this difficulty, one may consider forming a rectangle from 97.5% credible intervals, in effect implementing a Bonferroni correction. However, there is no guarantee that the resulting rectangle will respect the two-dimensional analogue to (5). In other words, some points inside the rectangle may be less likely than some points outside. Allowing for a possibly non-rectangular confidence set is one among several challenges in extending our technique to a vector of nanoparticle characteristics. As such, we leave this extension to future research.

Acknowledgements. This material is based upon work supported by the National Science Foundation under Grant No. DMS-0706857. Any opinions, findings, and conclusions or recommendations expressed in this material are those of the authors and do not necessarily reflect the views of the National Science Foundation. We thank two anonymous reviewers for

constructive suggestions that improved this work.

Appendix

This Appendix provides additional details regarding the numerical studies of Section 4.

Detailed assumptions for agglomeration patterns. Agglomerated nanoparticles were assumed to arise from four equally likely geometric configurations: triangles (60% three particles with one particle on top of the other two, 30% six particles with the previous three-particle configuration on top of three other particles, 10% ten particles with the previous six-particle configuration on top of four other particles), squares (60% four particles with a layer of two particles on top of another layer of two particles, 30% nine particles with three layers of three particles each, 10% sixteen particles with four layers of four particles each), vertical chains with particles on top of each other (60% two particles, 30% three particles, 10% four particles), and horizontal chains with particles next to but not on top of each other (60% two particles, 30% three particles, 10% four particles). Visual illustrations of these configurations appear in Figure 1 of Charnigo et al (2007).

Implementation details for compound estimation. The compound estimation procedure of Charnigo and Srinivasan (2011a, 2011b) was applied with local fitting degree $J = 7$, 27 centering points, and convolution parameter $\beta = 12$ following filtration and extrapolation preprocessing with extrapolation parameter $\kappa = 0.2$ and convolution parameter $\beta = 120$. Local constant and slope estimates were obtained using smoothing splines of degree 7 with 12 knots in the interval $[0, 180]$. Coefficents of higher-order local fits were calculated using inductive estimates with bandwidth parameters $h_2 = h_3 = 1/150$ and $h_4 = h_5 = h_6 = h_7 = 1/30$.

References

[1] Agarwal, B.M. and Mengüç, M.P. (1991). Forward and inverse analysis of single and multiple-scattering of collimated radiation in an axisymmetrical system. *International Journal of Heat and Mass Transfer*, **34**, 633–647.

[2] Arridge, S.R. (1999). Optical tomography in medical imaging. *Inverse Problems*, **15**, R41–R93.

[3] Atwater, H.A. and Polman, A. (2010). Plasmonics for improved photovoltaic devices. *Nature Materials*, **9**, 205–213.

[4] Bohren, C. and Huffman, D. (1998). *Absorption and Scattering of Light by Small Particles*. Wiley, New York.

[5] Cai, W. and Shalaev, V. (2010). *Optical Metamaterials: Fundamentals and Applications*. Springer, New York.

[6] Casella, G. and Berger, R. (2002). *Statistical Inference*, Second Edition. Duxbury, Pacific Grove.

[7] Catchpole, K.R. and Polman, A. (2008). Plasmonics solar cells. *Optics Express*, **16**, 21793–21800.

[8] Charnigo, R., Francoeur, M., Kenkel, P., Mengüç, M.P., Hall, B., and Srinivasan, C. (2011). Estimating quantitative features of nanoparticles using multiple derivatives of scattering profiles. *Journal of Quantitative Spectroscopy and Radiative Transfer*, **112**, 1369–1382.

[9] Charnigo, R., Francoeur, M., Mengüç, M. P., Brock, A., Leichter, M., and Srinivasan, C. (2007). Derivatives of scattering profiles: tools for nanoparticle characterization. *Journal of the Optical Society of America A*, **24**, 2578–2589.

[10] Charnigo, R. and Srinivasan, C. (2011a). Self-consistent estimation of mean response functions and their derivatives. *Canadian Journal of Statistics*, **39**, 280–299.

[11] Charnigo, R. and Srinivasan, C. (2011b). On simultaneous estimation of a mean response and its derivatives. Submitted for publication. Available at {www.richardcharnigo.net/TechReports}.

[12] Daun, K.J., Stagg, B.J., Liu, F., Smallwood, G.J., and Snelling, D.R. (2007). Determining aerosol particle size distributions using time-resolved laser-induced incandescence. *Applied Physics B*, **87**, 363–372.

[13] Devroye, L. and Lugosi, G. (2001). *Combinatorial Methods in Density Estimation*. Springer, New York.

[14] DiMatteo, R.S., Greiff, P., Finberg, S.L., Young-Waithe, K.A., Choy, H.K.H., Masaki, M.M., and Fonstad, C.G. (2001). Enhanced photogeneration of carriers in a semiconductor via coupling across a nonisothermal nanoscale vacuum gap. *Applied Physics Letters*, **79**, 1894–1896.

[15] Fernandez, G. (2003). *Data Mining using SAS Applications*. Taylor & Francis, New York.

[16] Francoeur, M., Vaillon, R., and Mengüç, M. P. (2011). Thermal aspects on the performance of nanoscale-gap thermophotovoltaic power generators, *IEEE Transactions on Energy Conversion*, **26**, 686–698.

[17] Francoeur, M., Venkata, P. G., and Mengüç, M. P. (2007). Sensitivity analysis for characterization of gold nanoparticles and 2D agglomerates via surface plasmon scattering patterns. *Journal of Quantitative Spectroscopy and Radiative Transfer*, **106**, 44-55.

[18] Gelman, A., Carlin, J., Stern, H., and Rubin, D. (1995). *Bayesian Data Analysis*. Chapman & Hall/CRC, Boca Raton.

[19] Gu, X., Ren, K., Masciotti, J., and Hielscher, A.H. (2009). Parametric image reconstruction using the discrete cosine transform for optical tomography. *Journal of Biomedical Optics*, **14**, 064003.

[20] Hastie, T., Tibshirani, R., and Friedman, J. (2001). *The Elements of Statistical Learning*. Springer, New York.

[21] Kim, H.K., Lee, J.H., and Hielscher, A.H. (2010). PDE-constrained fluorescence tomography with the frequency-domain equation of radiative transfer. *IEEE Journal of Selected Topics in Quantum Electronics*, **16**, 793–803.

[22] Laroche, M., Carminati, R., and Greffet, J.J. (2006). Near-field thermophotovoltaic energy conversion. *Journal of Applied Physics*, **100**, 063704.

[23] Loader, C. (1999). *Local Regression and Likelihood*. Springer, New York.

[24] Manickavasagam, S., and Mengüç, M. P. (1997). Scattering matrix elements of fractal-like soot agglomerates. *Applied Optics*, **36**, 1337–1351.

[25] Mengüç, M. P. and Manickavasagam, S. (1993). Inverse radiation problem in axisymmetric cylindrical media. *AIAA Journal of Thermophysics and Heat Transfer*, **7**, 479–486.

[26] Muller, D., Kolgotin, A., Mattis, I., Petzold, A., and Stohl, A. (2011). Vertical profiles of microphysical particle properties derived from inversion with two-dimensional regularization of multiwavelength Raman lidar data: experiment. *Applied Optics*, **50**, 2069–2079.

[27] Nishizawa, T., Sugimoto, N., Matsui, I., Shimizu, A., and Okamoto, H. (2011). Algorithms to retrieve optical properties of three component aerosols from two-wavelength backscatter and one-wavelength polarization lidar measurements considering nonsphericity of dust. *Journal of Quantitative Spectroscopy and Radiative Transfer*, **112**, 254–267.

[28] Park, K., Basu, S., King, W.P., and Zhang, Z.M. (2008). Performance analysis of near-field thermophotovoltaic devices considering absorption distribution. *Journal of Quantitative Spectroscopy and Radiative Transfer*, **109**, 305–316.

[29] Ripley, B. D. (1996). *Pattern Recognition and Neural Networks*. Cambridge University Press, Cambridge.

[30] Venkata, P. G., Aslan, M. M., Mengüç, M. P., and Videen, G. Surface plasmon scattering by gold nanoparticles and two-dimensional agglomerates (2007). *ASME Journal of Heat Transfer*, **129**, 60–70.

[31] Videen, G., Aslan, M. M., and Mengüç, M. P. (2005). Characterization of metallic nanoparticles via surface wave scattering: A. Theoretical framework. *Journal of Quantitative Spectroscopy and Radiative Transfer*, **93**, 195–206.

[32] Whale, M.D. (1997). A fluctuational electrodynamics analysis of microscale radiative heat transfer and the design of microscale thermophotovoltaic devices. Ph.D. Thesis, Massachusetts Institute of Technology, Cambridge MA.

[33] Zhao, Q., Zhou, J., Zhang, F., and Lippens, D. (2009). Mie resonance-based dielectric metamaterials. *Materials Today*, **12**, 60–69.

Table 1: Below is a glossary of notation introduced in this manuscript. The column "Definition" supplies a brief definition, while the column "Location" identifies the location in the manuscript where the notation is introduced.

Notation	Definition	Location
$\mathbf{Y} = (Y_1, \ldots, Y_n)^T$	random variables representing potential experimental outcomes	§2.1, ¶1
$f(\mathbf{y}; u)$	probability density function identifying likely/unlikely outcomes	§2.1, ¶1
$\mathbb{R}^n$	n-dimensional space	§2.1, ¶1
A	generic subset of $\mathbb{R}^n$	§2.1, ¶1
u	parameter representing nanoparticle characteristic of interest	§2.1, ¶2
$\mathbf{y} = (y_1, \ldots, y_n)^T$	realized values of random variables ("data")	§2.1, ¶2
$\bar{y}$	sample mean	§2.1, ¶3
$pr(u)$	prior probability density function for u	§2.2, ¶1
$\mathbb{R}$	real numbers	§2.2, ¶1
B	generic subset of $\mathbb{R}$	§2.2, ¶1
$po(u; \mathbf{y})$	posterior probability density function for u	§2.2, ¶2
I	generic credible interval for u	§2.2, ¶4
inf, sup	infimum (greatest lower bound), supremum (least upper bound)	§2.2, ¶5
$t(\mathbf{y})$	sufficient statistic	§2.3, ¶1
$g(t(\mathbf{y}); u)$	part of $f(\mathbf{y}; u)$ that depends on u	§2.3, ¶1
$h(\mathbf{y})$	part of $f(\mathbf{y}; u)$ that does not depend on u	§2.3, ¶1
M	number of auxiliary data sets	§3.3.1 ¶2
$\mu(u)$	mean vector in normal approximation to $f(\mathbf{y}; u)$	§3.3.2 ¶1
$\Sigma(u)$	covariance matrix in normal approximation to $f(\mathbf{y}; u)$	§3.3.2 ¶1

Det	determinant of a matrix	§3.3.2 ¶1
$\widetilde{t}(\mathbf{y})$	dimension-reduced quantity treated like a sufficient statistic	§3.3.3 ¶1
$D(\mathbf{y}; c)$	discrepancy between $M_{33}(\theta; \mathbf{y})$ and $M_{33;c}(\theta)$	§3.3.3 ¶2
θ	far field angle in scattering experiment	§3.3.3 ¶3
$M_{33}(\theta; \mathbf{y})$	estimated scattering matrix entry (nanoparticle characteristic unknown)	§3.3.3 ¶3
$M_{33;c}(\theta)$	estimated scattering matrix entry (nanoparticle characteristic known)	§3.3.3 ¶4
$M'_{33}(\theta; \mathbf{y})$	derivative of $M_{33}(\theta; \mathbf{y})$ with respect to θ	§3.3.3 ¶4
$M'_{33;c}(\theta)$	derivative of $M_{33;c}(\theta)$ with respect to θ	§3.3.3 ¶4
$g(\widetilde{t}(\mathbf{y}); u)$	proxy for $g(t(\mathbf{y}); u)$	§3.3.3 ¶6
$\nu(u)$	mean vector in normal approximation to $g(\widetilde{t}(\mathbf{y}); u)$	§3.3.3 ¶6
$\Lambda(u)$	covariance matrix in normal approximation to $g(\widetilde{t}(\mathbf{y}); u)$	§3.3.3 ¶6
dim	dimension of a vector	§3.3.3 ¶6
C	set of possible values for nanoparticle characteristic of interest	§3.3.5 ¶2
$a_0, a_1, \ldots, a_k$	endpoints of small intervals constituting C	§3.3.5 ¶2
$N_0, N_1, \ldots, N_k$	numerator of $po(u; \mathbf{y})$ evaluated at small interval endpoints	§3.3.5 ¶3
τ	permutation that sorts $N_0, N_1, \ldots, N_k$	§3.3.5 ¶3
m	number of small intervals constituting credible interval	§3.3.5 ¶4
$\mathbf{y}_{33,u,rep}$	data sets generated for numerical study	§4.1.2 ¶1
$11, 12, 33, 34$	identifiers of row and column in scattering matrix	§4.1.2 ¶3
rep	number of data sets generated for numerical study	§4.1.2 ¶5
$\mathbf{y}^{aux}_{33,u,rep}$	auxiliary data sets generated for numerical study	§4.1.3 ¶4
$\widetilde{t}(\mathbf{y}_{33,u,rep})$	dimension-reduced quantity from data set $\mathbf{y}_{33,u,rep}$	§4.1.4 ¶1
$po(u; \mathbf{y}_{33,u,rep})$	posterior probability density function from data set $\mathbf{y}_{33,u,rep}$	§4.1.4 ¶1
$I_{\mathbf{y}_{33,u,rep}}$	credible interval from data set $\mathbf{y}_{33,u,rep}$	§4.1.5 ¶1
$\mathcal{I}$	indicator function	§4.1 ¶4

Figure 1:

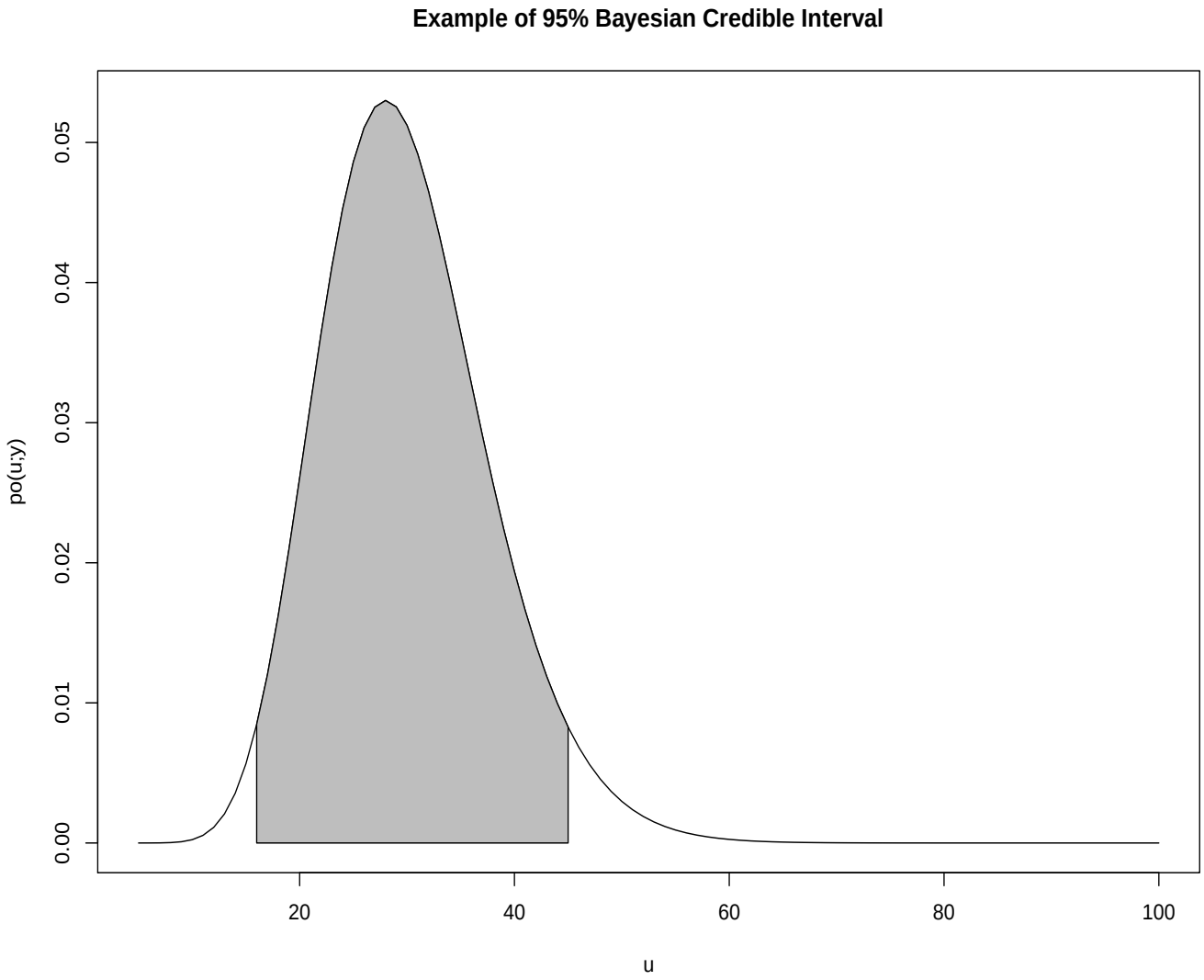

The curve is a posterior probability density function $po(u; \mathbf{y})$. The shaded area under $po(u; \mathbf{y})$ from $u = 16$ to $u = 45$ equals 95%, and thus $u = 16$ to $u = 45$ defines a 95% Bayesian credible interval.

Figure 2:

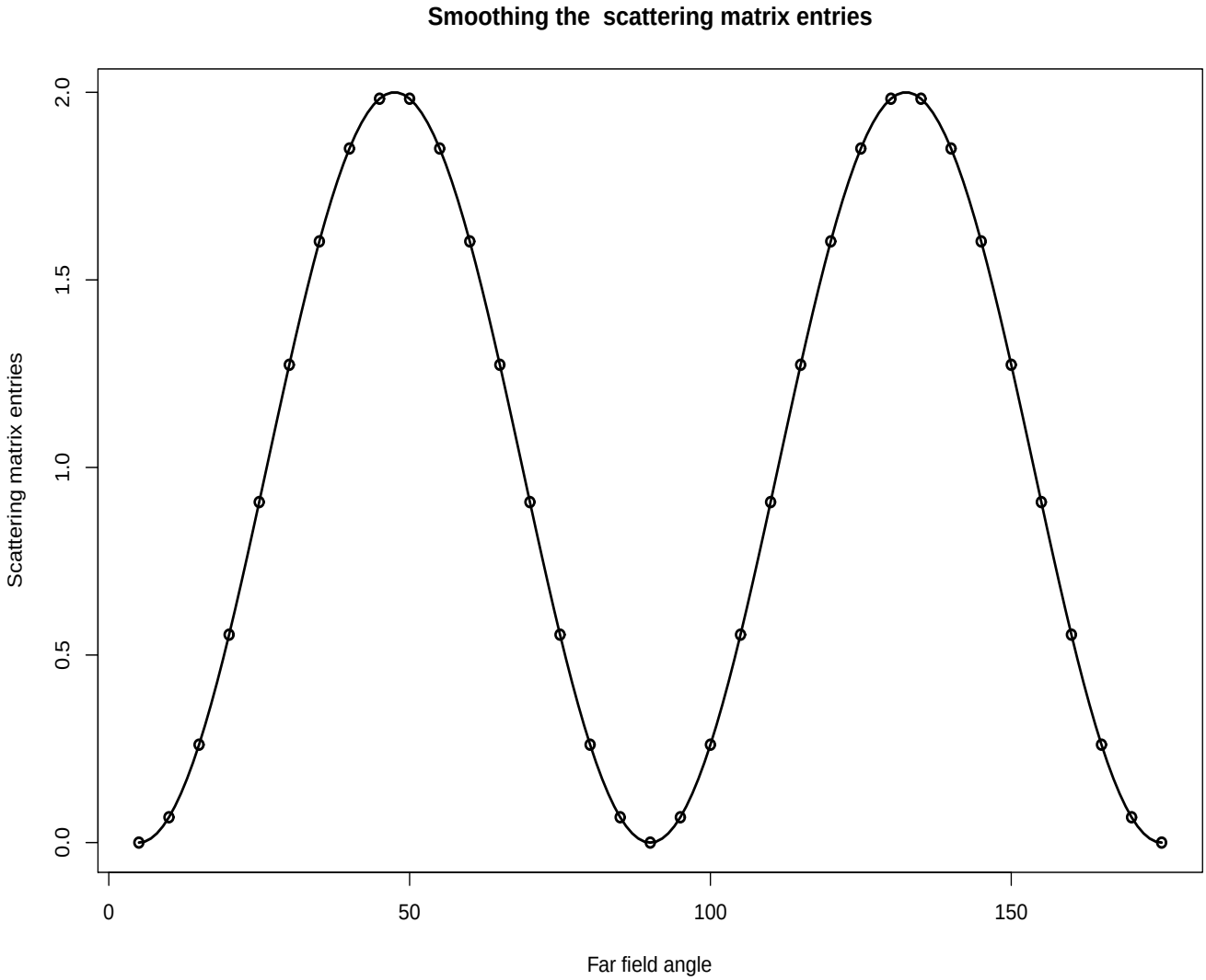

The points indicate the scattering matrix entries $y_1, y_2, \ldots, y_{35}$ corresponding to far field angles of $5, 10, \ldots, 175$. (We chose a sparse grid of far field angles to make this plot legible.) The curve, denoted $M_{33}(\theta; \mathbf{y})$ in the text, is a smoothed version of the scattering matrix entries.

Figure 3:

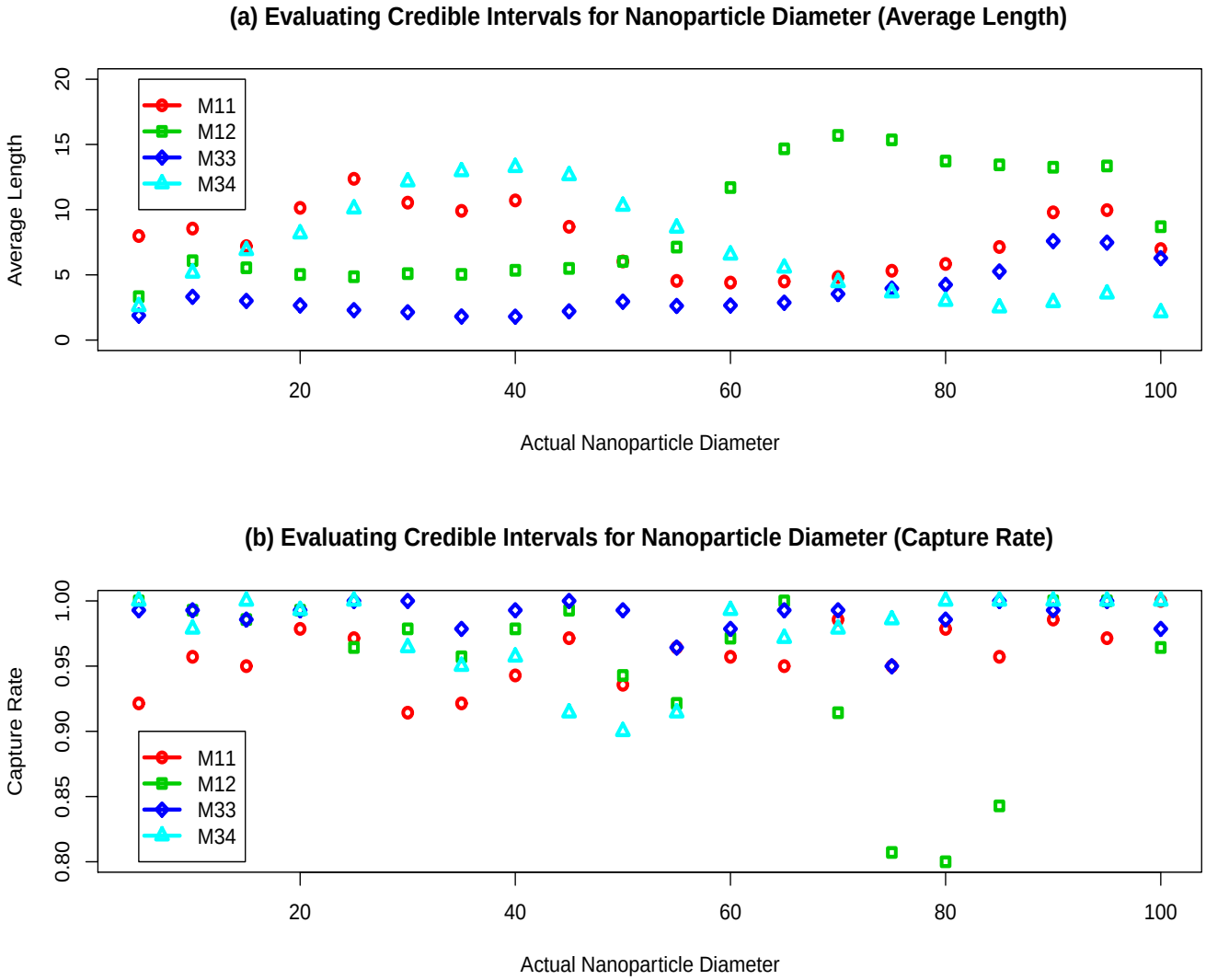

Panel (a) shows the average length of the 140 credible intervals constructed in our first numerical study at each nanoparticle diameter $(5, 10, \ldots, 100$ nm) and row/column combination of the scattering matrix (11, 12, 33, 34) from which entries were taken to define data sets. Panel (b) depicts the fraction of the 140 credible intervals that captured the actual nanoparticle diameter.

Figure 4:

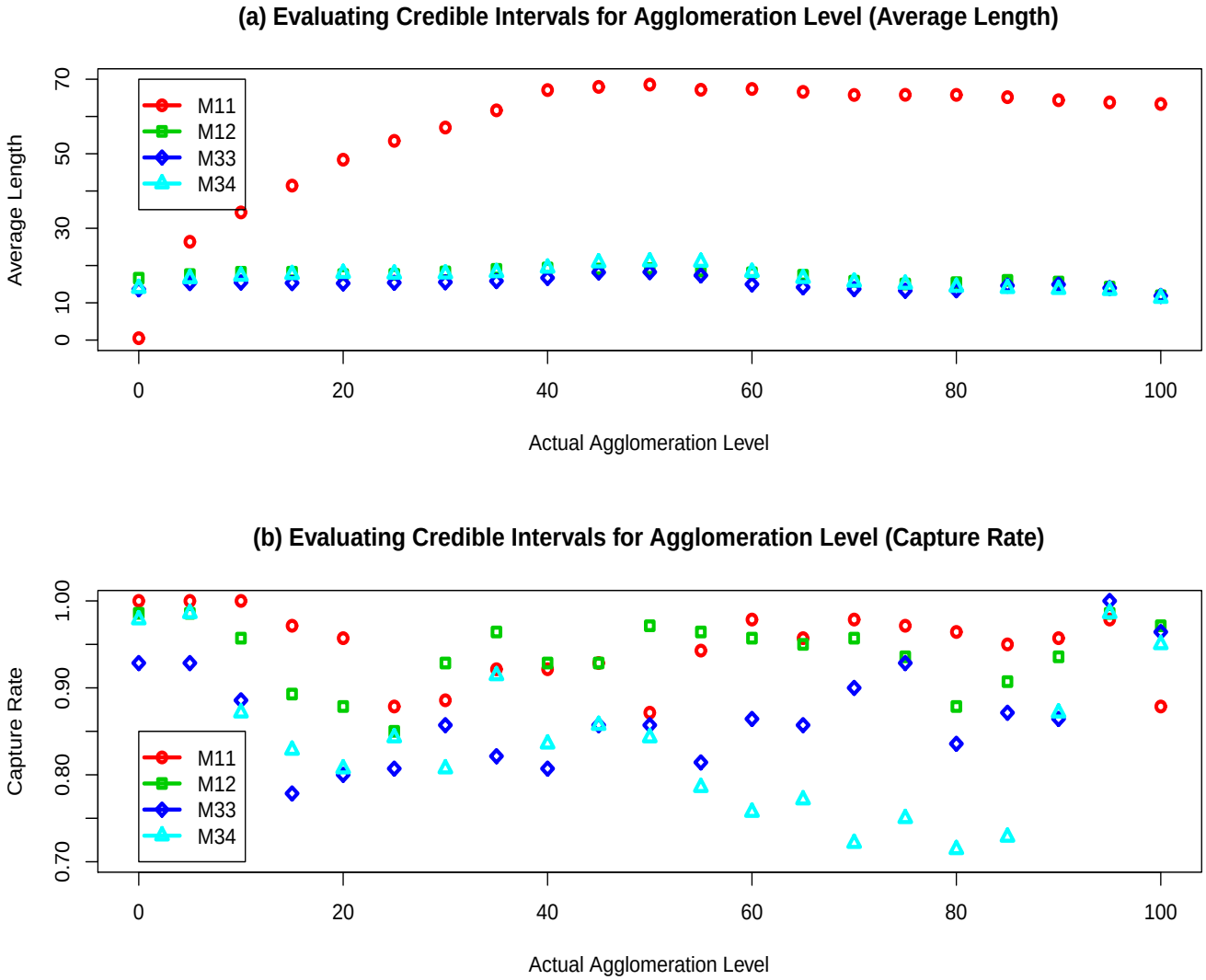

Panel (a) shows the average length of the 140 credible intervals constructed in our second numerical study at each agglomeration level $(0, 5, \ldots, 100$ percent) and row/column combination of the scattering matrix (11, 12, 33, 34) from which entries were taken to define data sets. Panel (b) depicts the fraction of the 140 credible intervals that captured the actual agglomeration level.